Two-dimensional mixture of amphiphilic dimers and spheres: Self-assembly behaviour

Santi Prestipino, Gianmarco Munaò, Dino Costa, Giuseppe Pellicane, and Carlo Caccamo

Citation: The Journal of Chemical Physics **147**, 144902 (2017); doi: 10.1063/1.4995549
View online: http://dx.doi.org/10.1063/1.4995549
View Table of Contents: http://aip.scitation.org/toc/jcp/147/14
Published by the American Institute of Physics

Two-dimensional mixture of amphiphilic dimers and spheres: Self-assembly behaviour

Santi Prestipino,[1,a)] Gianmarco Munaò,[1,2] Dino Costa,[1] Giuseppe Pellicane,[3,b)] and Carlo Caccamo[1]

[1]*Dipartimento di Scienze Matematiche e Informatiche, Scienze Fisiche e Scienze della Terra, Università degli Studi di Messina, Viale F. Stagno d'Alcontres 31, 98166 Messina, Italy*
[2]*Dipartimento di Chimica e Biologia "Adolfo Zambelli," Università di Salerno, Via Giovanni Paolo II 132, 84084 Fisciano, SA, Italy*
[3]*School of Chemistry and Physics, University of Kwazulu-Natal, Private Bag X01, Scottsville 3209, Pietermaritzburg, South Africa*

(Received 12 July 2017; accepted 24 September 2017; published online 11 October 2017)

The emergence of supramolecular aggregates from simple microscopic interaction rules is a fascinating feature of complex fluids which, besides its fundamental interest, has potential applications in many areas, from biological self-assembly to smart material design. We here investigate by Monte Carlo simulation the equilibrium structure of a two-dimensional mixture of asymmetric dimers and spheres (disks). Dimers and disks are hard particles, with an additional short-range attraction between a disk and the smaller monomer of a dimer. The model parameters and thermodynamic conditions probed are typical of colloidal fluid mixtures. In spite of the minimalistic character of the interaction, we observe—upon varying the relative concentration and size of the two colloidal species—a rich inventory of mesoscale structures at low temperature, such as clusters, lamellæ (i.e., polymer-like chains), and gel-like networks. For colloidal species of similar size and near equimolar concentrations, a dilute fluid of clusters gives way to floating lamellæ upon cooling; at higher densities, the lamellæ percolate through the simulation box, giving rise to an extended network. A crystal-vapour phase-separation may occur for a mixture of dimers and much larger disks. Finally, when the fluid is brought in contact with a planar wall, further structures are obtained at the interface, from layers to branched patterns, depending on the nature of wall-particle interactions. *Published by AIP Publishing.*
https://doi.org/10.1063/1.4995549

I. INTRODUCTION

Colloids are mixtures in which insoluble particles in the submicron range are dispersed throughout another substance (the "medium") of lower molecular weight. Besides being common in everyday life, colloidal suspensions provide the template by which the building blocks of biological matter (ultimately, cells) are constructed; hence, they are extensively studied by biologists and chemists.

From the point of view of physics, colloids are versatile materials with a rich self-assembly behaviour,[1–5] which in the fluid regime includes a wealth of different structures—such as micelles, lamellæ, networks, and clusters. In the last decades, the constant increase in computing power has been pivotal in revealing similar features also in simple models of colloids, where the medium is only implicit and interactions are simplified to the bone, showing that also these systems are capable of self-organization. In particular, there are by now many examples of model colloids and colloidal mixtures (i.e., with two or more solute species) where diffuse order arises from local interactions, without the guidance of any external agent.[6–13] The ability to control self-assembly is of overwhelming importance in the fabrication of synthetic colloids tailored for targeted applications,[14,15] such as the delivery of drugs in the human body[16–18] or the addition of bioactive substances to foods.[19,20]

Recently, we have investigated by Monte Carlo simulation the low-temperature structure of a dilute mixture of dimers (made up of two spherical monomers of unequal size) and spheres.[21–23] In these studies, an additional attraction takes place between spheres and the small monomers. This model aims to represent, within an implicit-medium description, a colloidal dispersion made up of a guest species and an amphiphilic dimer where the small monomer is lyophobic and has a strong affinity for the guest. Originally, our model interaction was intended for driving the formation of capsules of spheres coated with dimers (as in Refs. 24 and 25). Indeed, we have seen encapsulation in simulation runs at low concentration of spheres. However, in different conditions of size and concentrations, other aggregates arise in equilibrium, including clusters, lamellæ, and liquid-vapour phase separation. Clearly, a minimalistic model of mixture makes it simpler to identify the microscopic features (sizes and interactions) that superintend the formation of specific patterns at equilibrium, so that the model can be designed on purpose, i.e., to obtain a target structure just by thermalization.

[a)]Author to whom correspondence should be addressed: sprestipino@unime.it
[b)]Also at: National Institute for Theoretical Physics (NITheP), KZN node, Pietermaritzburg, South Africa.

Significantly enough, real colloids can be engineered with the same characteristics as our model, implying that the self-assembly behaviour of the latter can also be probed experimentally.[26,27]

In this paper, we study by Monte Carlo simulation the two-dimensional (2D) counterpart of the model in Refs. 22 and 23, focusing on its self-assembly behaviour at low temperature. The broad interest in 2D colloidal models is witnessed by a flourishing literature on this topic, aimed at exploring routes to self-assembly into structures of assigned morphology. In most cases, particles have been modeled either through repulsive pair potentials[28–33] or as patchy particles,[34–38] both being known for giving stable cluster phases at moderate temperatures. Often, the focus has been on the possibility to create quasicrystalline solids by spontaneous aggregation of the particles; in one instance,[39] the solid phases of a 2D mixture of disks and patchy particles have been analyzed, reporting the existence of many crystalline and quasicrystalline patterns; on the other hand, in a just published paper,[40] a mixture of Janus particles and much smaller disks has been studied for increasing densities, highlighting the existence of an intermediate gel-like regime. We argue that each of these studies deserves its own interest since it provides suggestions that can be helpful for a better understanding of the three-dimensional case.

The models employed in Refs. 28–38 are one-component systems, and the interest has been exclusively (with the only exception of Refs. 30 and 38) in the solid phases. Hence, the main novelty of our work is that we investigate self-organization in a more complex two-component mixture, concentrating on the fluid sector of the phase diagram. Moreover, as a convenient benefit of studying a 2D system, experience has shown that relaxation to equilibrium in three dimensions may take a very long time, a circumstance which sheds uncertainty on the stability of the observed structures. Working in 2D provides a possible way out since this permits to overcome the limitations of a slow approach to equilibrium.

We anticipate that the phenomenology of a 2D mixture of dimers and spheres (disks) is quite rich. Aggregates of various kinds are found, depending on the concentration and size of disks. At low density and for disks of the same size as the large monomers, clusters are observed at moderate temperatures, giving way to one-dimensional lamellæ (polymers) and vesicles (closed polymers) upon cooling, at least for nearly equimolar conditions. Under the same conditions of concentration, at moderate density a percolating network of lamellæ is formed. We have also investigated the effect of increasing the size of disks at fixed density: when the disk diameter is large enough, a distinct crystal-vapour separation occurs at sufficiently low concentration. Other characteristic patterns arise when bringing the mixture against an attractive wall, a situation that mimics the bias exerted by an external substrate or template on the self-assembly process. In this case, the crucial parameter is the strength of the attraction.

The outline of the paper is as follows. After describing the model and the simulation method in Sec. II, we present and discuss our results in various settings in Sec. III. Finally, concluding remarks and perspectives are given in Sec. IV.

II. MODEL AND METHOD

The model is the 2D counterpart of the mixture studied in Refs. 22 and 23: a dimer is made up of two tangent hard disks of unequal size, with diameters σ_1 and $\sigma_2 = 3\sigma_1$, whereas guest particles are represented as hard disks of size $\sigma_3 \geq \sigma_2$. Besides hard repulsion, we put an additional pair attraction between species 1 and 3, modeled as a square-well potential of depth ε. The width of the well is set equal to the size σ_1 of the smallest species. By creating contacts with two nearby disks, a small monomer provides the bridge by which the disks can bind together. In the following, σ_2 and ε are taken as units of length and energy, respectively (reduced quantities are denoted with an asterisk). Finally, N_1 and N_3 are the number of dimers and disks, respectively; hence, $N = N_1 + N_3$ is the total number of particles and $\chi = N_3/N$ is the disk concentration.

Most of the data have been collected for $N_3 = 400$ disks and for mixtures with $\sigma_3 = \sigma_2$. The overall number density in reduced units has been fixed to $\rho^* \equiv (N/A)\sigma_2^2 = 0.05$ (where A is the system area), but we have also performed a few runs at $\rho^* = 0.25$. We have analyzed the system behaviour at five concentrations: χ = 20%, 33%, 50%, 67%, and 80%. Once ρ^* and χ are fixed, the number of dimers follows accordingly. Furthermore, we have examined how self-assembly changes when, still for $\rho^* = 0.05$, the diameter of disks is increased up to $5\sigma_2$. In Table I, we summarize the packing fractions of disks and dimers for all the cases investigated at $\rho^* = 0.05$. The thermodynamic conditions (low density) and model parameters (short-range attraction and diameter ratios) have been so chosen as to represent, within an implicit-medium description, a generic colloidal dispersion made up of a guest species and

TABLE I. Sizes and concentrations of disks, with ensuing packing fractions of disks ($\eta_{\rm disk}$) and dimers ($\eta_{\rm dim}$) for the cases investigated in this work at $\rho^* = 0.05$.

	χ = 20%		χ = 33%		χ = 50%		χ = 67%		χ = 80%	
σ_3/σ_2	$\eta_{\rm disk}$	$\eta_{\rm dim}$	$\eta_{\rm disk}$	$\eta_{\rm dim}$	$\eta_{\rm disk}$	$\eta_{\rm dim}$	$\eta_{\rm disk}$	$\eta_{\rm dim}$	$\eta_{\rm disk}$	$\eta_{\rm dim}$
1	0.007 854	0.034 90	0.013 09	0.029 09	0.019 63	0.021 86	0.026 18	0.014 54	0.031 42	0.008 72
2	0.031 42	0.034 90	0.052 36	0.029 09	0.078 54	0.021 86				
3	0.070 69	0.034 90	0.117 8	0.029 09	0.176 7	0.021 86				
4	0.125 7	0.034 90	0.209 4	0.029 09	0.314 2	0.021 86				
5	0.196 3	0.034 90	0.327 2	0.029 09	0.490 9	0.021 86				

an amphiphilic dimer where the small monomer is lyophobic and has a strong affinity for the guest.

Simulations are carried out using the standard Metropolis algorithm in the canonical ensemble, with periodic conditions at the boundaries of a square box. Depending on the temperature T, from a few to several hundred million Monte Carlo (MC) cycles have been performed, one cycle consisting of N trial single-particle (either translational or rotational) moves. The schedule of moves is so designed that detailed balance holds exactly. The maximum random shift and rotation are adjusted during the equilibration run so as to keep the ratio of accepted to total number of moves close to 50%. As a general setup, particles are initially distributed at random in the simulation box; then, after setting the reduced temperature $T^* \equiv k_B T/\epsilon$ at either 0.15 or 0.10, the MC simulation is started. In a previous study,[22] we had checked that using as initial condition the configuration obtained at the end of a slow cooling process from high temperature does not make any substantial difference in the structural properties of the ensuing steady state, even when the state probed is located inside a spinodal region. This is due to the fact that the simulated systems are overall dilute. We surmise that the same will occur also in two dimensions.

The property that better indicates how far away the system is from equilibrium is the total potential energy U: an energy fluctuating around a fixed value for long is the hallmark of (meta)stable equilibrium. At any instant, U gives the number of 1-3 contacts present in the system configuration. Hence, a stationary energy value indicates that the aggregates have eventually acquired a nearly stable structure. Once equilibrium (or a steady state whatsoever) has been reasonably established, we compute the radial distribution function (RDF) $g_{33}(r)$ of disks in a rather long production run of 2×10^8 cycles. Even in a strongly heterogeneous system, where mesoscopic structures are present, $g_{33}(r)$ bears valuable information on the disk arrangement in the immediate neighbourhood of a reference disk. Other instruments to gain insight into the system structure are visual inspection and cluster analysis. As for the latter, we identify at regular times—and count as a function of the number of hosted disks—all connected structures, generically referred to as "clusters" of disks held together by dimers. We classify two disks as bound together when their distance is smaller than $r_{\min} = \sigma_3 + 3\sigma_1$; we refer the reader to Sec. III for a detailed discussion about this point.

The statistics of clusters have been gathered from the last 2×10^8 cycles of the MC trajectory and are updated every 1000 cycles. The cluster-size distribution, $N_{\rm cl}(s)$, has been normalized according to the expression[23,41–44]

$$n(s) = \frac{sN_{\rm cl}(s)}{N_3}, \qquad (1)$$

where s is the cluster size, defined as the number of disks within the cluster (hence, an isolated disk is a cluster of size one). The function $n(s)$ represents the average fraction of particles contained in all clusters of size s, as opposed to the mean number $N_{\rm cl}(s)$ of s-clusters in one configuration. Next, for each cluster, we have counted the number $N_{\rm dim}$ of dimers belonging to it and computed the binding energy E_b (that is, the number of 1-3 contacts). Insofar as the number of dimers bound to a disk is on average the same for each disk in a cluster, we expect that the distributions $N_{\rm dim}(s)$ and $E_b(s)$ are strongly correlated to each other. Finally, we determine the distribution of the number z of disks that are bound to the same disk in the sense specified above and the distribution of the angle α formed by two 3-3 bonds with an end in common.

III. RESULTS

A. A wide variety of structures

In Fig. 1, we report the evolution of U in MC time for $\sigma_3 = \sigma_2$, at two temperatures, 0.15 and 0.10 and various disk concentrations χ; the overall density has been set equal to $\rho^* = 0.05$. We see that, after an initial exponential decay, U enters a regime of much slower relaxation which can last long at the lowest temperature; however, even in the worst case, relative to $\chi = 20\%$, a stationary state is attained after, say, 5×10^8 MC cycles. Looking at Fig. 1, it appears that the absolute value of U/N_3 grows as concentration decreases, meaning that the more numerous are dimers relative to disks, the more contacts each disk can establish with small monomers. The higher value of U/N_3 for larger χ is a symptom of the lesser stability (and more marked dynamic nature) of the structures formed as the concentration of disks is increased.

We get a first clue about the nature of the structures present in the system by visual inspection (see Fig. 2). For $T^* = 0.15$, the system can invariably be described as a fluid of small globular clusters [panels (a)-(e)]. The nature of aggregates is more varied for $T^* = 0.10$: these are capsules for $\chi = 20\%$ [Fig. 2(f)] or lower, while the shape is more elongated and worm-like

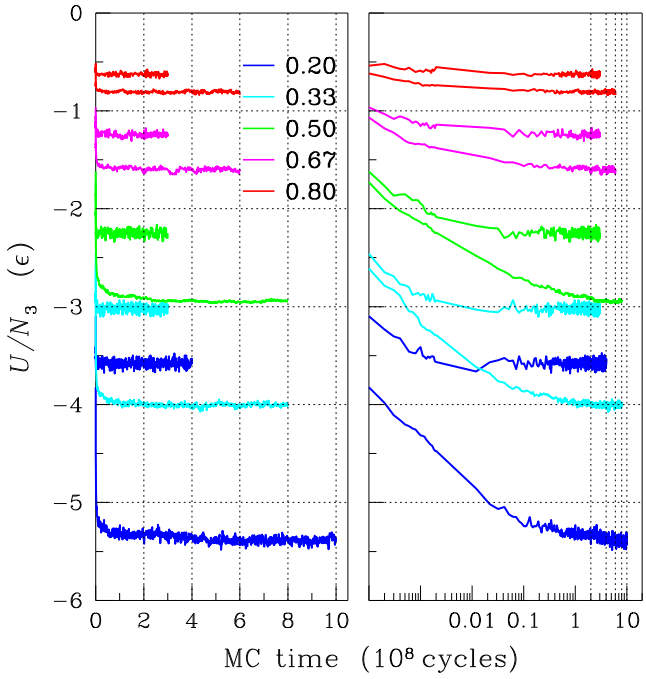

FIG. 1. Left: MC evolution of the potential energy U per disk, for $\rho^* = 0.05$ and various χ values (in the legend). For each color, two curves are shown, relative to two temperatures: $T^* = 0.15$ (above) and 0.10 (below). Right: same data reported on a semi-logarithmic scale. The energy relaxation during the first 10^7 cycles is appreciable on the right panel.

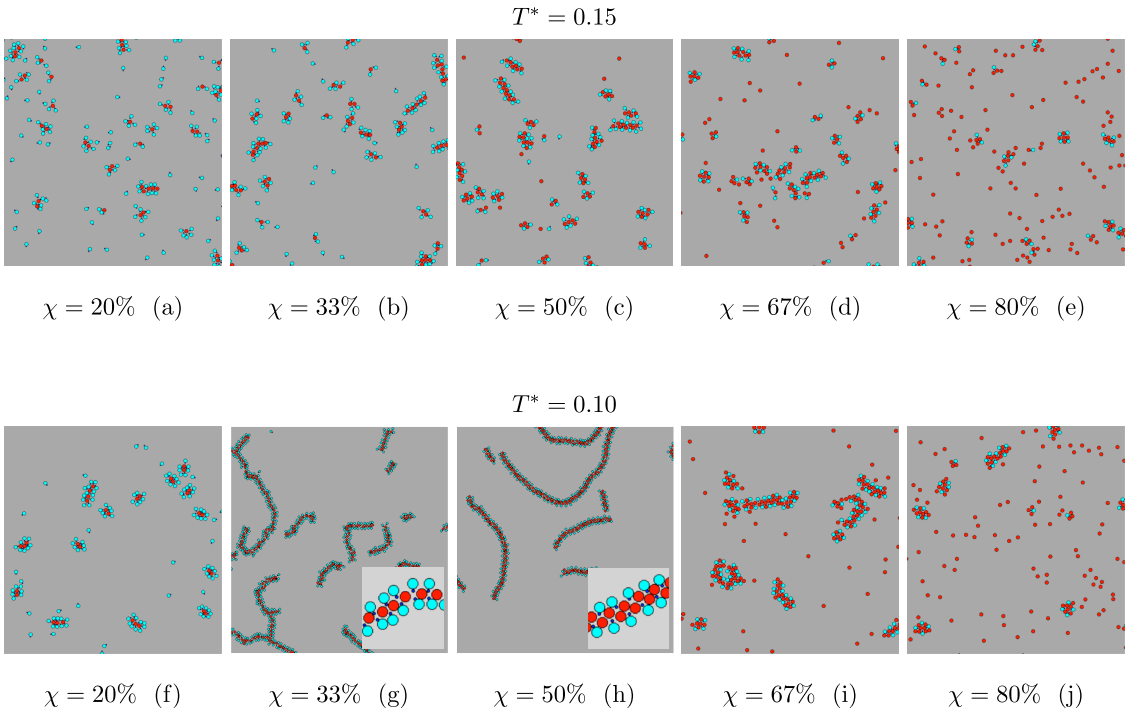

FIG. 2. Snapshots of typical steady-state configurations for $\rho^* = 0.05$ (only a fraction of the system is shown). Different colors are used for the three species: blue (1), cyan (2), and red (3).

for intermediate concentrations [Figs. 2(g) and 2(h)]. A closer look at such "worms" reveals that they are assembled from a seamlessly repeating unit, like in a homopolymer chain. For the highest χ considered, the mean size of aggregates again reduces since there are too few dimers, and many disks then remain isolated [Figs. 2(i) and 2(j)]. Therefore, it turns out that a large numerical disequilibrium between dimers and disks is detrimental to aggregation; in other words, aggregates only achieve large sizes when the number of disks roughly matches that of dimers.

For $T^* = 0.10$, the general criterion underlying the specific shape of aggregates is energy minimization, whereas entropic considerations play a less important role. Clearly, the relative size of the particles is a crucial parameter (see Sec. III B), as would also be the range of 1-3 attraction. The short range assumed is responsible for the essentially one-dimensional character of the larger structures formed. Particularly interesting are the cases $\chi = 33\%$ and $\chi = 50\%$ [Figs. 2(g) and 2(h)], where the typical aggregate (a worm) is the 2D analog of a lamella. The geometry of its backbone is dictated by the necessity to keep the energy small while complying with the given concentration: as illustrated in the insets of Figs. 2(g) and 2(h), this is accomplished by a straight chain of disks for $\chi = 33\%$ ($U/N_3 = -4$ and $\alpha \simeq 180°$) and a zig-zag chain for $\chi = 50\%$ ($U/N_3 = -3$ and $\alpha \simeq 90°$). Both chain morphologies allow disks to bind all dimers, so that no free particles are eventually left in the box. Occasionally, a worm bends to the point that a closed loop appears, which is nothing but a 2D vesicle (see two examples in Fig. 3, both relative to $\chi = 50\%$). This indicates that worms/lamellæ have a high flexibility, suggesting that their bending modulus is small. From a thermodynamic perspective, the presence in the system of numerous lamellar aggregates hints at a phase-separation scenario in equilibrium where the competing phases are a dilute fluid and a lamellar solid (i.e., the 2D analog of the situation depicted in Fig. 8 of Ref. 7).

It is worth spending a few words on the specificity of aggregate formation in the present model. During the initial stages of thermalization, aggregation through the formation of contacts between disks and dimers is very fast. As an aggregate grows in size, however, its surface becomes increasingly rich in large monomers, which are inert particles; at a certain point, the aggregate stops growing since its disks and small monomers (which would provide the "fuel" for further growth) all lie beneath the surface. Once in a while, two large aggregates succeed to join together and U then makes a small step downwards. Indeed, while local adjustments of the structure occur at a high rate, the merging of large disconnected aggregates (a phenomenon akin to coarsening) only takes place on much longer time scales. The existence of two regimes of growth (fast and slow), corresponding to a transition from diffusion-limited to reaction-limited aggregation (see, e.g., Ref. 45),

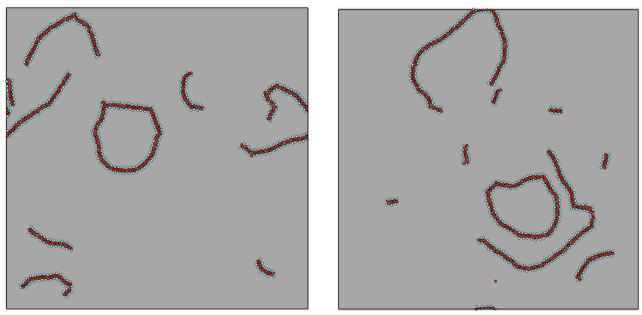

FIG. 3. Two snapshots of the mixture for $\rho^* = 0.05$, $T^* = 0.10$, and $\chi = 50\%$, where vesicles (closed lamellae) are clearly visible.

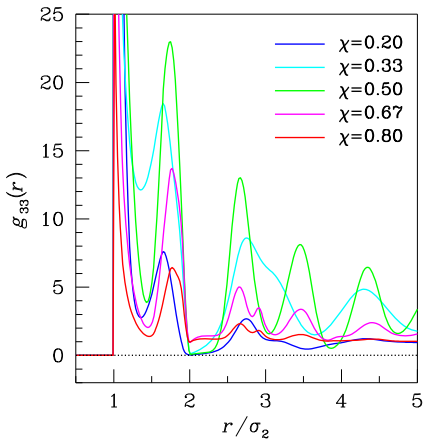

FIG. 4. RDF of disks with diameter $\sigma_3 = \sigma_2$ at $\rho^* = 0.05$, for $T^* = 0.10$ and various concentrations (in the legend).

is reflected in the crossover of U from an exponential to a sub-exponential decay, as seen in Fig. 1.

The structure of the mixture has been so far discussed through an examination of a few snapshots. Now, we give a more comprehensive treatment in terms of size and energy distributions of clusters (where the term "cluster" is used here in the broad sense, as a synonym of aggregate). As anticipated in Sec. II, two disks form a bound pair when their distance is less than $r_{\min} = \sigma_3 + 3\sigma_1$: this is the maximum distance at which two disks can still be in contact with the same small monomer (exactly placed in the middle). For $\sigma_3 = \sigma_2$, this implies that a disk makes bonds with all first and second neighbours, identified as such through the RDF profile—see Fig. 4, where $g_{33}(r)$ is plotted for $T^* = 0.10$ and all concentrations. We note that the use of a smaller $r_{\min}$ would imply to often break long linear clusters in pieces which, by eye, are clearly connected; hence, we keep our choice at the cost of slightly overestimating the tail of the cluster-size distribution as a result of accidental closeness of two aggregates (anyway, an unlikely possibility at low densities).

In Fig. 5, we plot the normalized cluster-size distribution $n(s)$, see Eq. (1). Overall, the results are similar to those found in three dimensions:[22] for $T^* = 0.10$ (top panel), $n(s)$ has gaps for large s at moderate concentrations, indicating a low propensity of the largest aggregates to add/lose particles. In particular, for $\chi = 50\%$, a broad maximum is visible for $s \approx 100$, while the smaller the mean size of clusters, the more we deviate from equimolarity. Hence, we confirm that the biggest aggregates occur at moderate concentration. The noise present in the cluster-size distribution at large s would clearly be reduced by increasing the size of the system. For fixed sample size, the statistical accuracy of $n(s)$ substantially improves with increasing temperature; concurrently, the typical cluster size decreases (bottom panel); all curves for $\chi \geq 33\%$ show a maximum around $s = 2$-6, as expected for a fluid of small clusters.[43,44] Next, we report in Fig. 6 the mean number $N_{\rm dim}(s)$ of dimers hosted in a s-cluster as well as the mean number $E_{\rm b}(s)$ of 1-3 contacts. It turns out that the number of dimers per cluster is linearly dependent on s for large s, suggesting a nearly constant density of dimers within the big clusters. Also the binding energy $E_{\rm b}(s)$ grows linearly with size, moreover exhibiting a strong correlation with $N_{\rm dim}(s)$.

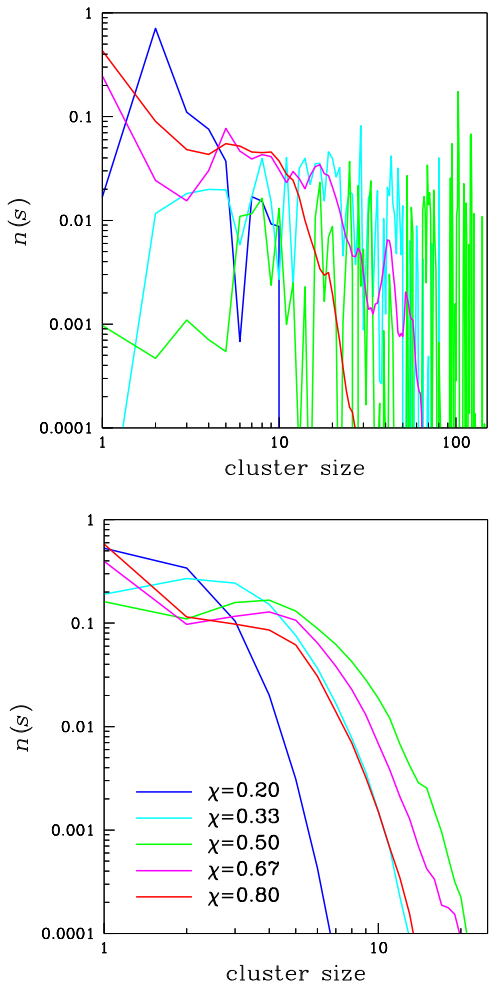

FIG. 5. Normalized cluster-size distribution $n(s)$ for $\sigma_3 = \sigma_2$ and $\rho^* = 0.05$ (χ values in the legend): $T^* = 0.10$ (top) and $T^* = 0.15$ (bottom).

As geometrical indicators of the arrangement of disks within clusters, we have computed (i) the distribution $P(\alpha)$ of the angle α formed by two 3-3 bonds with a common disk at the angle vertex and (ii) the statistics of the disk coordination number z (defined in Sec. II). In Fig. 7, results are presented for

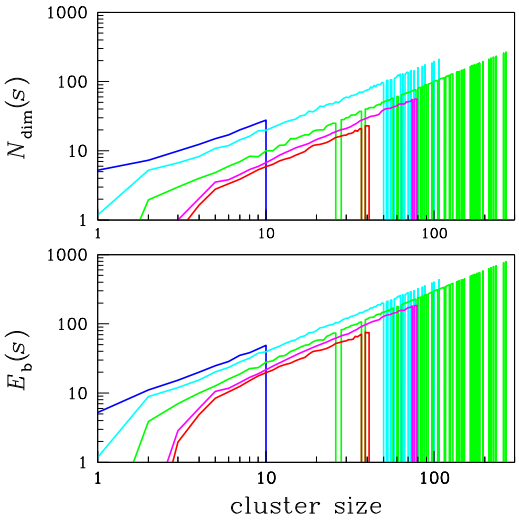

FIG. 6. Average number of dimers (top) and of 1-3 contacts (bottom) in a cluster, for $T^* = 0.10$ (same color code as in Fig. 5).

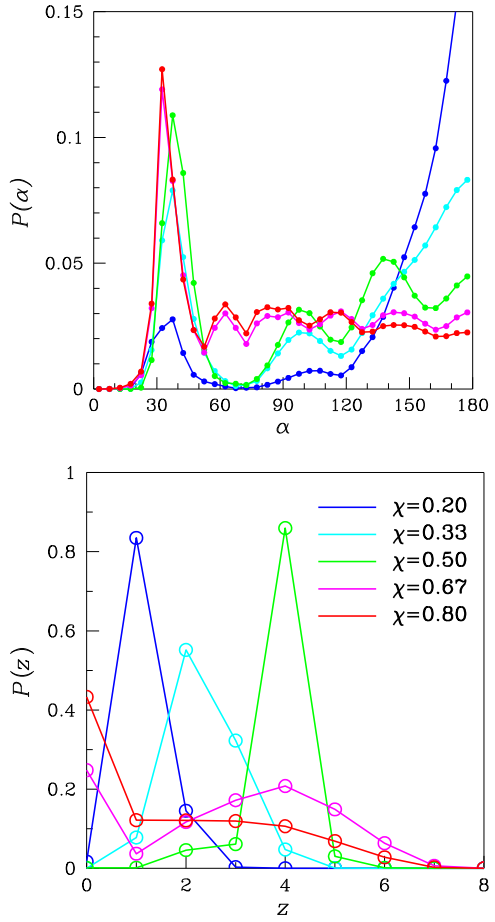

FIG. 7. Top: distribution of the angle α between two closest 3-3 bonds, for $T^* = 0.10$ and various concentrations (same legend as in the panel below). Bottom: distribution of the disk coordination number z.

all concentrations, at the lower temperature only ($T^* = 0.10$). For $\chi = 67\%$ and 80%, $P(\alpha)$ is essentially uniform and the sharp maximum near 30° refers to the typical angle between a first-neighbour bond and a second-neighbour bond [see Figs. 2(i) and 2(j)]; for $\chi = 50\%$, the maxima of $P(\alpha)$ roughly fall at multiples of 45°, which is consistent with zig-zagging of disks within worms. Upon moving to $\chi = 33\%$, the maximum at 180° undergoes a sharp enhancement due to a different geometry of disk chains at this χ (i.e., straight rather than zig-zag). Finally, for $\chi = 20\%$, very few clusters have a size larger than two, and most of them are straight chains. A glance at Fig. 7(b) confirms the above picture. The most likely value of z is four for $\chi = 50\%$ and two for $\chi = 33\%$. The pronounced maximum

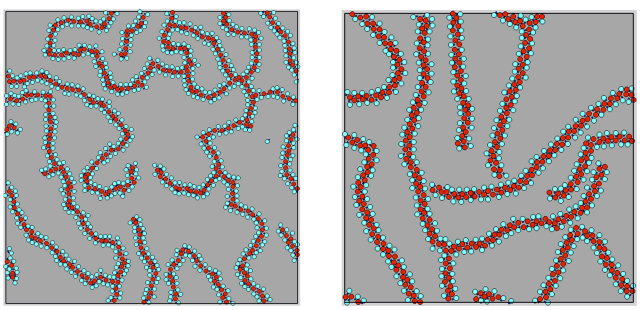

FIG. 8. Two snapshots of the mixture with density $\rho^* = 0.25$ and temperature $T^* = 0.10$, for $\chi = 33\%$ (left) and $\chi = 50\%$ (right).

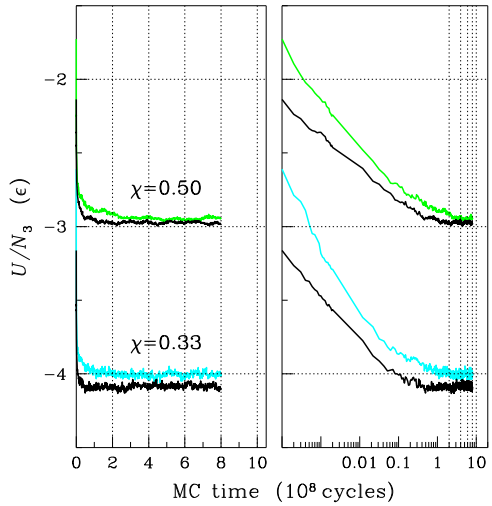

FIG. 9. Left: MC evolution of the potential energy U per disk, for $T^* = 0.10$ and two χ values. For each concentration, two curves are shown, relative to two densities: $\rho^* = 0.05$ (above, in color) and 0.25 (below, black). Right: same data reported on a semi-logarithmic scale.

of $P(z)$ at zero reaffirms the presence of many isolated disks when χ is large.

As to the dependence of self-assembly on density, we have studied the mixture with $\sigma_3 = \sigma_2$ at $\rho^* = 0.25$, while still keeping the temperature fixed at 0.10. In this case, even longer lamellæ are formed for $\chi = 33\%$ and 50%, but due to a denser environment they are now joined in an intricate manner, giving rise to an extended network (Fig. 8). Now the asymptotic energy is slightly less than for $\rho^* = 0.05$ since lamellar order is more diffuse (see Fig. 9). Looking at Fig. 8, we note in both panels the presence of a spanning cluster (i.e., a connected structure with at least one particle on each side of the box), which is a remarkable outcome considering that this structure has emerged from scratch through the blind, undirected MC dynamics. By taking the snapshot of the mixture at intervals of a few ten million cycles, we see that the disk network is completely reshuffled at each shot, suggesting that it is all but rigid. Clearly, a detailed assessment of the statistical properties of the percolating network would require specialized scale-free schemes to get rid of finite-size effects, such as those involving the estimate of the fractal dimension of the largest aggregate occurring in the mixture (see, e.g., Ref. 46).

B. Increasing the disk size

In this section, we examine self-assembly as a function of disk diameter, still for $\rho^* = 0.05$ and $T^* = 0.10$ (to speed up simulations, for $\chi = 20\%$ and $\chi = 33\%$ we have used smaller samples of $N_3 = 200$ disks). We increase σ_3/σ_2 in unit steps, up to reaching five. Clearly, as σ_3 grows, the packing fraction of disks becomes progressively larger, and even a mixture of density 0.05 may appear quite dense. On the other hand, the main stimulus to study samples with varying σ_3 is to establish whether ordered patterns exist that are unknown to mixtures with $\sigma_3 = \sigma_2$; in that respect, a moderate increase in packing fraction can help, rather than hinder, the discovery of novel self-organizing behaviour.

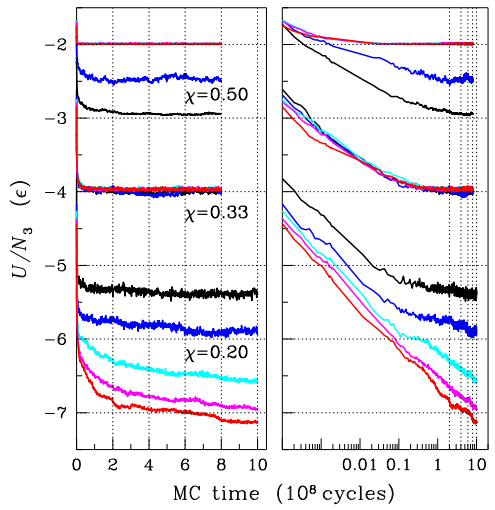

FIG. 10. Left: MC evolution of the potential energy U per disk, for $\rho^* = 0.05$, three concentrations, and various σ_3/σ_2 values (1, black; 2, blue; 3, cyan; 4, magenta; 5, red). Right: same data reported on a semi-logarithmic scale.

We first comment on the time evolution of U, reported in Fig. 10 for three values of χ. What first catches the eye is the slowness of the approach to equilibrium for the lowest concentration considered, i.e., $\chi = 20\%$. As is apparent from the semi-logarithmic plots, even after one billion of MC cycles the mixture has not yet reached a stationary state, a problem that worsens with increasing σ_3. However, the decrease of U in time appears to be intermittent, suggesting that only small (i.e., local) adjustments of the structure occur most of the time, occasionally interrupted by a major system rearrangement (such as the coalescence of two large aggregates). This means that, after approximately 10^8 MC cycles, the dynamics of the mixture has eventually entered a coarsening regime which would hardly affect the intermediate-scale order already established. Hence, it is worthless to extend the runs further. A second observation concerns the asymptotic value of U/N_3 as a function of σ_3. We see that the sequence is reversed when going from $\chi = 20\%$ to $\chi = 50\%$, meaning that, while for $\chi = 20\%$ the number of 1-3 contacts per disk becomes larger with increasing σ_3, a bigger disk size is indifferent ($\chi = 33\%$), if not even deleterious ($\chi = 50\%$) to lamellar order.

These expectations are confirmed by looking at the system snapshots (see Fig. 11). For $\chi = 50\%$, worms/lamellæ are already absent for $\sigma_3/\sigma_2 = 2$, and only small clusters are formed; for larger σ_3, the mixture even becomes more homogeneous. With two dimers per disk ($\chi = 33\%$), lamellar order locally survives though in an overall entangled structure where lamellæ are either braided into small necklaces ($\sigma_3/\sigma_2 = 2$ or 3) or connected in a gel-like network ($\sigma_3/\sigma_2 = 5$); in both cases, the number of 1-3 contacts is on average four per disk. The intermediate $\sigma_3/\sigma_2 = 4$ case shows intermediate features between 3 and 5.

The most interesting case by far is the one relative to $\chi = 20\%$. Again, for $\sigma_3/\sigma_2 = 2$, interlinked chains of particles are found. As σ_3 grows, the disk structure becomes more compact, and many squares, pentagons, and hexagons appear, where disks are held together by the dimers interspersed between them. The guests are now so big that large monomers have no possibility to adequately screen the attraction between two nearby clusters during the fast-growth regime, and coagulation then continues until all particles are gathered in a unique condensate. Eventually, for $\sigma_3/\sigma_2 = 5$ mostly the squares survive and this motif propagates to large distances, giving rise to extended square-crystal patches. In this structure, an average of four dimers are entrapped in the hole inside each square, which corresponds to a reduced energy per disk of −8. The prevalent square symmetry of the system patches for $\sigma_3/\sigma_2 = 5$ is made evident in the location of the first

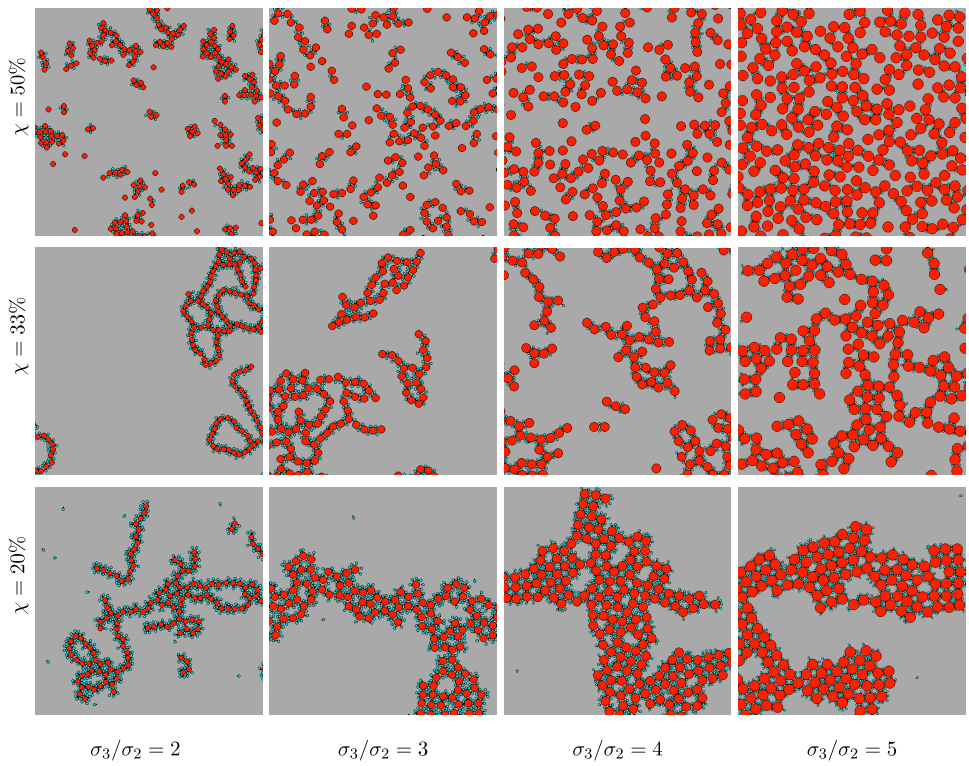

FIG. 11. Snapshots of long-term configurations for $\rho^* = 0.05$ and $T^* = 0.10$ (only a fraction of the system is shown).

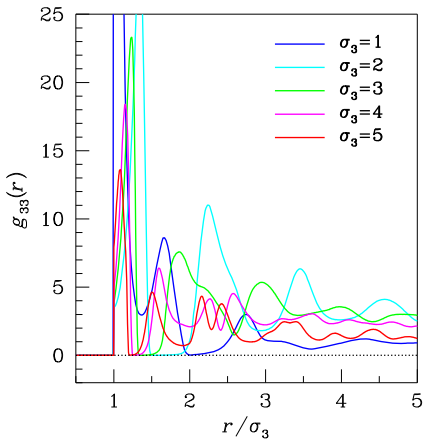

FIG. 12. RDF of disks with increasing diameter σ_3 (in the legend in units of σ_2), for $\rho^* = 0.05$, $T^* = 0.10$, and $\chi = 20\%$.

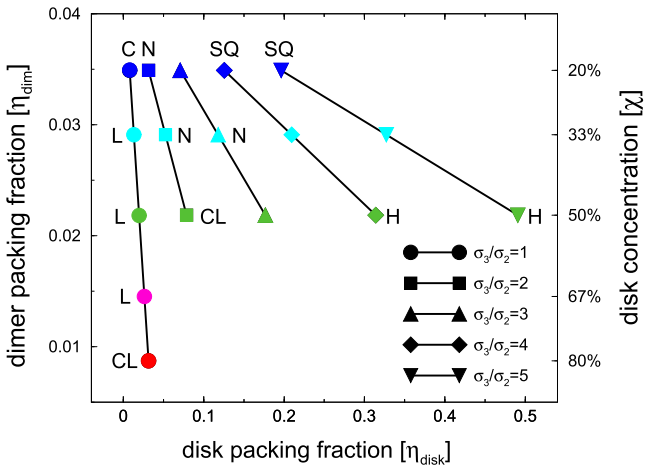

FIG. 13. Map of the self-assembled structures observed at $T^* = 0.10$ for various mixtures of density $\rho^* = 0.05$. The patterns found, upon varying η_{disk} and η_{dim}, are marked with a symbol: capsules (C), clusters (CL), homogeneous fluid (H), lamellæ (L), necklaces (N), and square crystal (SQ) coexistent with vapour. Dots with no attached marker refer to situations of difficult classification (see Fig. 11).

three peaks of $g_{33}(r)$, see Fig. 12: the second and the third peak are approximately centered at distances which are in a ratio of $\sqrt{2}$ and 2, respectively, with the location of the first peak. Also notice how the nearest-neighbour distance in units of σ_3 first grows when σ_3/σ_2 changes from 1 to 2 and then gradually reduces on increasing the disk size further, which is consistent with the transition of the system from compact capsules to more floppy configurations of disks, until a full-fledged crystalline structure eventually occurs. Obviously, the emergence from scratch of a two-component square crystal without defects is extremely unlikely in a simulation since this would require a perfectly coordinated movement of many particles. Hence, only a floating polycrystalline structure can be observed at finite time, which anyway well reflects the symmetry of the stable crystal phase at high density; indeed, the sub-exponential asymptotic decay of U corresponds to the extremely slow elimination of crystal defects (mainly grain boundaries and pores) from the condensate. From the point of view of thermodynamics, a polycrystalline structure in vacuum clearly points to a crystal-vapour coexistence scenario; this looks different from more conventional instances of two-phase separation where the morphologies of the minority-phase inclusion have a high symmetry (see, e.g., Refs. 47–50).

The present results can be compared with those in Ref. 39, where a mixture of disks and patchy particles with two to five patches is studied. At relatively high packing fractions, various types of solid-vapour separations have been reported at low temperature, similarly as found in our 20% mixture. Lamellæ and gel-like structures—but no crystal states—arise in another recent simulation study[40] though the relative size of amphiphilic particles and disks is the opposite of ours. A comparison with other works in 2D[28–38] is harder since the models employed are one-component systems and the interest has been almost exclusively in the solid phases rather than in the fluid sector of the phase diagram.

In conclusion, the number of dimers per disk proves crucial to decide whether a dilute mixture of dimers and large disks orders in space. The different outcomes obtained at different concentrations suggest that, in order to separate guest particles (disks) from the solvent, the addition of a consistent amount of amphiphilic dimers could be helpful. We summarize the results up to now in Fig. 13, where we give an overview of the self-organized structures observed for $\rho^* = 0.05$ as a function of the packing fractions of disks (η_{disk}) and dimers (η_{dim}):

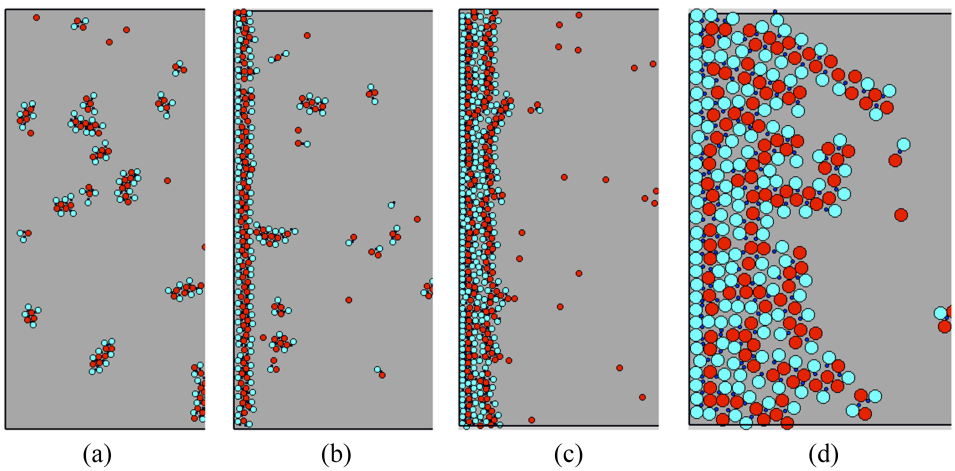

FIG. 14. Snapshots of typical stationary configurations for inhomogeneous mixtures with $\chi = 50\%$ and $T^* = 0.15$ (the number of disks is $N_3 = 400$; only the situation near the left wall is shown, whereas boundary conditions are periodic along the y direction): (a) hard walls ($\rho^* = 0.05$); (b) attractive hard walls ($\rho^* = 0.05, \epsilon_W^* = 2$, and $h_W^* = 1$); (c) attractive hard walls ($\rho^* = 0.05, \epsilon_W^* = 5$, and $h_W^* = 3$); (d) attractive hard walls ($\rho^* = 0.25, \epsilon_W^* = 5$, and $h_W^* = 3$).

linear aggregates are observed for low $\eta_{\rm disk}$ and moderate $\eta_{\rm dim}$ values, while crystal-vapour separation only occurs for large $\eta_{\rm disk}$ and $\eta_{\rm dim}$.

C. Mixtures under confinement

Our last effort has been a study of the structure of the equimolar mixture with $\sigma_3 = \sigma_2$ under a number of inhomogeneous conditions. We fix the temperature at $T^* = 0.15$ and the overall density at $\rho^* = 0.05$; moreover, we take a rectangular simulation box, with sides L_x and L_y in the ratio 3:1 and periodic conditions along the y direction. As before, the initial configuration of the mixture is fully disordered; subsequently, it is taken to evolve under the Metropolis algorithm until U ceases to drift.

Initially, we assume the box sides orthogonal to x ("walls") to be unstructured and impenetrable [Fig. 14(a)]. In this case, we have verified (by computing the x-dependent and species-resolved number densities) that a depletion region, poor of particles, of width $\approx 4\sigma_2$ occurs in the long run near $x = 0$ and $x = L_x$, as an effect of the entropic repulsion associated with lateral confinement of elongated objects. The depletion region is still present at high temperature, but its width is smaller (see Fig. 15), suggesting that the strength of the entropic repulsion exerted by the wall is enhanced by the formation of aggregates. Then, while still keeping the walls rigid, we add an exponential attraction u_W between each wall and the *large* monomers only (which would mimic walls with a strong affinity for species 2). Specifically, for the left wall, $u_W(x) = -\epsilon_W \exp(-x/h_W)$. In this case, the confining potential heavily interferes with the intrinsic self-assembly properties of the system, and novel structures may be expected to result. Two cases are considered: $\epsilon_w = 2\epsilon$, $h_W = \sigma_2$ (b) and $\epsilon_W = 5\epsilon$, $h_W = 3\sigma_2$ (c). In case (b) (weak, short-range attraction), a monolayer of disks wets each wall, sandwiched between two rows of dimers. For a stronger and longer-range attraction, layering is more effective [see Fig. 14(c)], though less and less perfect as the distance from the wall increases. The last examined case, (d), is identical to (c) but for the value of the number density, $\rho^* = 0.25$, instead of 0.05. The stationary structure of the mixture is now more strongly influenced by the interplay between diffusion (as referred to the MC, rather than Newtonian, dynamics) and drift in a dense environment. In the early stages of relaxation, the wall attraction determines a flow of dimers towards the walls. A number of disks are randomly captured in this flow, but the region near the walls is so crowded that the system structure cannot be optimized by diffusion alone and, as a result, layering does not occur in an ordered fashion. In the end, an arrested structure arises near the walls [Fig. 14(d)], with arm-like protrusions towards the interior of the box. Similar (dendritic) structures are found in the ballistic deposition of patchy particles on a substrate,[51] an irreversible process of adsorption which may vaguely recall the dynamics of our mixture after quenching.

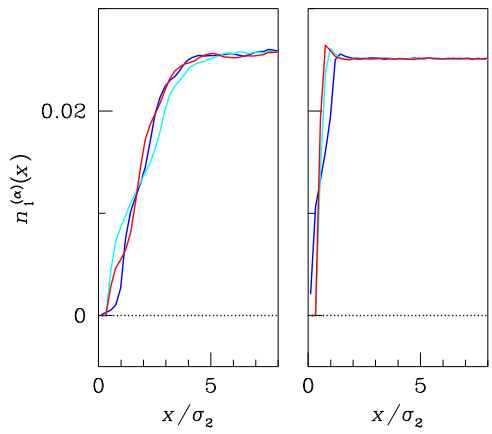

FIG. 15. One-body density functions for our model mixture under confining hard walls, for $\rho^* = 0.05$ and $\chi = 0.50$: $T^* = 0.15$ (left) and $T^* = 1.50$ (right). The color distinguishes the three species (1, blue; 2, cyan; and 3, red).

IV. CONCLUSIONS

Colloidal mixtures are smart materials, capable of countless self-organizing behaviours. In this paper, we have investigated by Monte Carlo simulation the self-assembly of a dilute 2D mixture made up of asymmetric dimers and disks. All interactions are hard-core, with an additional short-range square-well attraction between each disk and the smaller monomer of a dimer.

We have studied the long-time behaviour of the mixture, as a function of density and disk concentration, for a wide range of disk diameters. At low temperature (one tenth in reduced units or less), a dilute mixture minimizes its energy by self-assembling into mesoscale structures. Specifically, for disks with the same diameter as large monomers, we find either small globular or long worm-like (lamellar) aggregates at low density, depending on the disk concentration; for sufficiently large densities, worms join together, giving rise to a spanning network. For larger disk sizes, the exact amount of dimers is crucial to decide whether the solution separates into crystal and vapour phases or it remains homogeneous altogether. For instance, when the ratio between the numbers of dimers and disks is 4:1 and the size of disks is at least four times that of large monomers, a unique condensate of disks occurs, locally resembling a square crystal. Other ordering patterns (i.e., layers and branched structures) arise when the mixture is confined between two attractive walls.

In the recent literature, many one-component systems, either with interparticle pair repulsions or made up of patchy particles, have been studied with the aim of exploring the nature of the solid phases, often focusing on the conditions allowing quasi-crystalline states. Our work instead provides insight into the fluid phase diagram and self-organization of a two-component mixture. The occurrence of a wide variety of mesoscale structures at low temperature, resembling those observed in realistic colloidal suspensions, stands as a highly non-trivial feature of our oversimplified model of mixture. As a further remark, we observe that the very same mixture of asymmetric dimers and disks can also be employed as a model of surfactant (the dimer) dispersed in an explicit solvent (the disk); in this case, realistic conditions would be those where the total packing fraction is liquid-like, and disks are more numerous and much smaller than dimers. In the next future, we plan to address the dynamics of self-assembly in our model, with specific attention to the nucleation and growth of lamellar structures.

[1] G. M. Whitesides and B. Grzybowski, Science **295**, 2418 (2002).
[2] G. M. Whitesides and M. Boncheva, Proc. Natl. Acad. Sci. U. S. A. **99**, 4769 (2002).
[3] M. Boncheva and G. M. Whitesides, MRS Bull. **30**, 736 (2005).
[4] J. N. Israelachvili, *Intermolecular and Surface Forces*, 3rd ed. (Academic Press, London, 1992).
[5] K. Thorkelsson, P. Bai, and T. Xu, Nano Today **10**, 48 (2015).
[6] J. A. Luiken and P. G. Bolhuis, Phys. Rev. E **88**, 012303 (2013).
[7] Z. Preisler, T. Vissers, F. Smallenburg, G. Munaò, and F. Sciortino, J. Phys. Chem. B **117**, 9540 (2013).
[8] T. Vissers, F. Smallenburg, G. Munaò, Z. Preisler, and F. Sciortino, J. Chem. Phys. **140**, 144902 (2014).
[9] G. Avvisati, T. Vissers, and M. Dijkstra, J. Chem. Phys. **142**, 084905 (2014).
[10] G. Munaò, P. O'Toole, T. S. Hudson, D. Costa, C. Caccamo, A. Giacometti, and F. Sciortino, J. Phys.: Condens. Matter **27**, 234101 (2015).
[11] J. M. Dempster and M. Olvera De La Cruz, ACS Nano **10**, 5909 (2016).
[12] L. B. Krott, C. Gavazzoni, and J. R. Bordin, J. Chem. Phys. **145**, 244906 (2016).
[13] P. O'Toole, A. Giacometti, and T. S. Hudson, Soft Matter **13**, 803 (2017).
[14] A. Yethiraj and A. van Blaaderen, Nature **421**, 513 (2003).
[15] Y. Wang, Y. Wang, D. R. Breed, V. N. Manoharan, L. Feng, A. D. Hollingsworth, M. Weck, and D. J. Pine, Nature **491**, 51 (2012).
[16] K. Kataoka, A. Harada, and Y. Nagasaki, Adv. Drug Delivery Rev. **47**, 113 (2001).
[17] M. N. Singh, K. S. Y. Hemant, M. Ram, and H. G. Shivakumar, Res. Pharm. Sci. **5**, 65 (2010).
[18] A. Kumari, R. Singla, A. Guliani, and S. K. Yadav, EXCLI J. **13**, 265 (2014).
[19] D. J. McClements, E. A. Decker, Y. Park, and J. Weiss, Crit. Rev. Food Sci. Nutr. **49**, 577 (2009).
[20] V. Dordević *et al.*, Food Eng. Rev. **7**, 452 (2015).
[21] G. Munaò, D. Costa, S. Prestipino, and C. Caccamo, Phys. Chem. Chem. Phys. **18**, 24922 (2016).
[22] S. Prestipino, G. Munaò, D. Costa, and C. Caccamo, J. Chem. Phys. **146**, 084902 (2017).
[23] G. Munaò, D. Costa, S. Prestipino, and C. Caccamo, Colloids Surf. A **532**, 397 (2017).
[24] W. Li, Y. Liu, G. Brett, and J. D. Gunton, Soft Matter **8**, 6027 (2012).
[25] R. Malik, J. Genzer, and C. K. Hall, Langmuir **31**, 3518 (2015).
[26] J. R. Wolters, J. E. Verweij, G. Avvisati, M. Dijkstra, and W. K. Kegel, Langmuir **33**, 3270 (2017).
[27] E. Bianchi, B. Capone, I. Coluzza, L. Rovigatti, and P. D. J. van Oostrum, Phys. Chem. Chem. Phys. **19**, 19847 (2017).
[28] T. Dotera, Isr. J. Chem. **51**, 1197 (2011).
[29] H. Pattabhiraman, A. P. Gantapara, and M. Dijkstra, J. Chem. Phys. **143**, 164905 (2015).
[30] B. Chacko, C. Chalmers, and A. J. Archer, J. Chem. Phys. **143**, 244904 (2015).
[31] H. G. Schoberth, H. Emmerich, M. Holzinger, M. Dulle, S. Förster, and T. Gruhn, Soft Matter **12**, 7644 (2016).
[32] M. Zu, P. Tan, and N. Xu, e-print arXiv:1703.08783.
[33] H. Pattabhiraman and M. Dijkstra, J. Phys.: Condens. Matter **29**, 094003 (2017).
[34] A. G. Vanakaras, Langmuir **22**, 88 (2006).
[35] M. N. van der Linden, J. P. K. Doye, and A. A. Louis, J. Chem. Phys. **136**, 054904 (2012).
[36] A. Reinhardt, F. Romano, and J. P. K. Doye, Phys. Rev. Lett. **110**, 255503 (2013).
[37] A. Reinhardt, J. S. Schreck, F. Romano, and J. P. K. Doye, J. Phys.: Condens. Matter **29**, 014006 (2017).
[38] R. A. Mathews K and E. Mani, e-print arXiv:1705.05321.
[39] E. Słyk, W. Rzysko, and P. Bryk, Soft Matter **12**, 9538 (2016).
[40] M. Borówko, W. Rzysko, S. Sokołowski, and T. Staszewski, J. Chem. Phys. **147**, 014904 (2017).
[41] D. Stauffer, Phys. Rep. **54**, 1 (1979).
[42] S.-H. Chen, J. Rouch, F. Sciortino, and P. Tartaglia, J. Phys.: Condens. Matter **6**, 10855 (1994).
[43] P. D. Godfrin, R. Castañeda-Priego, Y. Liu, and N. J. Wagner, J. Chem. Phys. **139**, 154904 (2013).
[44] P. D. Godfrin, N. E. Valadez-Pérez, N. J. Wagner, and Y. Liu, Soft Matter **10**, 5061 (2014).
[45] M. Y. Lin, H. M. Lindsay, D. A. Weitz, R. C. Ball, R. Klein, and P. Meakin, Nature **339**, 360 (1989).
[46] L. B. Partay, P. Jedlovszky, I. Brovchenko, and A. Oleinikova, J. Phys. Chem. B **111**, 7603 (2007).
[47] S. Prestipino, A. Laio, and E. Tosatti, J. Chem. Phys. **138**, 064508 (2013).
[48] S. Prestipino, A. Laio, and E. Tosatti, J. Chem. Phys. **140**, 094501 (2014).
[49] M. C. Abramo, C. Caccamo, D. Costa, P. V. Giaquinta, G. Malescio, G. Munaò, and S. Prestipino, J. Chem. Phys. **142**, 214502 (2015).
[50] A. Statt, P. Virnau, and K. Binder, Phys. Rev. Lett. **114**, 026101 (2015).
[51] N. A. M. Araújo, C. S. Dias, and M. M. Telo da Gama, J. Phys.: Condens. Matter **27**, 194123 (2015).